AAS 22-129

DEBRIS AVOIDANCE AND PHASE CHANGE MANEUVERS IN NEAR RECTILINEAR HALO ORBITS

Diane C. Davis,[*] Emily M. Zimovan-Spreen,[†] Stephen T. Scheuerle,[‡] and Kathleen C. Howell[§]

Over the course of its lifetime, Gateway may execute excursions from its baseline NRHO that include short-lead maneuvers to avoid other spacecraft or debris objects or long-lead rephasing within the NRHO to support rendezvous or other mission objectives. The dynamical characteristics of the NRHO are distinct from those of low Earth and low lunar orbits due to the simultaneous gravitational influences of the Earth and Moon. Thus, new approaches for executing debris avoidance maneuvers and rephasing maneuvers are necessary. The current investigation proposes methods for designing low-cost DAMs with short-lead planning time as well as rephasing maneuvers with many months of advance notice.

INTRODUCTION

The Gateway[1] is planned as a long-term outpost in deep space: a proving ground for deep space technologies and a staging location for missions to the lunar surface and beyond Earth orbit. The current baseline orbit for the Gateway is a Near Rectilinear Halo Orbit (NRHO) near the Moon.[2] The Gateway's NRHO satisfies many mission objectives and constraints, including low orbit maintenance costs and limited shadowing from eclipses. Planned excursions from the baseline NRHO may include transfers to other destinations in cislunar space and an ultimate transfer to an end-of-life orbit. Over the course of its lifetime, Gateway may also execute excursions from the baseline NRHO that are not currently planned in a mission manifest. Such unplanned transfers could include maneuvers to avoid other spacecraft or debris objects with limited advanced notice. Alternatively, long-lead rephasing within the NRHO to support rendezvous or other mission objectives may be necessary. The dynamical characteristics of the NRHO are distinct from those of low Earth and low lunar orbits due to the simultaneous gravitational influences of the Earth and Moon. Thus, new approaches for executing debris avoidance maneuvers (DAMs) and rephasing maneuvers are necessary. The current investigation explores methods for designing low-cost DAMs with short-lead planning time as well as rephasing maneuvers with many months of advance notice.

DYNAMICAL MODELS

The current investigation employs two dynamical models to describe the motion of the Gateway. The Circular Restricted 3-Body Problem (CR3BP) effectively describes the behavior of objects in and near the Gateway NRHO in a simplified framework that enables pattern definition and an understanding of the underlying dynamical flow. Then, an N-body model based on ephemeris data provides higher-fidelity analysis that incorporates the eccentricity of the Earth and Moon as well as the effects of solar gravity, allowing assessment of trajectory consistency across epochs.

[*] Principal Systems Engineer, a.i. solutions, Inc., 2224 Bay Area Blvd, Houston TX 77058, diane.davis@ai-solutions.com.
[†] Aerospace Engineer, Flight Mechanics and Trajectory Design Branch, NASA Johnson Space Center
[‡] Graduate Student, School of Aeronautics and Astronautics, Purdue University
[§] Hsu Lo Distinguished Professor, School of Aeronautics and Astronautics, Purdue University, Armstrong Hall of Engineering, 701 W. Stadium Ave., West Lafayette, IN 47907-2045, howell@purdue.edu. Fellow AAS; Fellow AIAA.

The Circular Restricted 3-Body Problem

The CR3BP describes the motion of a massless spacecraft affected by two primary gravitational bodies such as the Earth and the Moon. The model assumes that the two primary bodies are point masses orbiting their center of mass in circular orbits. The spacecraft moves freely under the influence of the two primaries, and its motion is described relative to a rotating reference frame. No closed-form solution exists to the CR3BP equations of motion, but five equilibrium solutions, the libration points, are denoted L_1 through L_5. Stable and unstable periodic orbit families, including the L_2 halo orbits, emerge in the vicinity of the libration points. For spacecraft orbiting in or near the Gateway NRHO, the Earth-Moon CR3BP delivers a good approximation for the trajectory and relative behaviors.

The N-Body Ephemeris Model and Error Modeling

To confirm the CR3BP results in a higher-fidelity model, N-body differential equations and planetary ephemerides are employed. The N-body dynamics describe the motion of a spacecraft in an inertial frame relative to a central body under the gravitational influence of the central body and additional perturbing bodies. Within this analysis, the relative position of each perturbing body with respect to the central body is instantaneously computed by employing NAIF SPICE ephemeris data. The Moon is selected as the central body for numerical integration in the J2000 inertial frame. The Earth and Sun are included as point masses, and the Moon's gravity is modeled using the GRAIL (GRGM660PRIM) model truncated to degree and order 8. Solar radiation pressure (SRP) acting on a sphere is also included in the force model.

For multi-revolution propagations in the NRHO, orbit maintenance (OM) maneuvers are implemented.[3] Operational errors on the spacecraft are incorporated in the higher-fidelity modeling as gaussian errors with zero mean and 3σ values as follows. Each OM maneuver is associated with a navigation error on the spacecraft state of 1 km in position and 1 cm/s in velocity. Maneuver execution errors comprising 1.5% in magnitude and 1° in direction, as well as a fixed magnitude of 1.42 mm/s, are applied to each OM maneuver. Mismodeling in SRP assumptions provide 15% error in area and 30% error in coefficient of reflectivity. Momentum wheel desaturations are assumed to occur once per revolution near apolune with a translational Δv component of 3 cm/s applied in a random direction.

BASELINE NRHO AND ORBIT MAINTENANCE

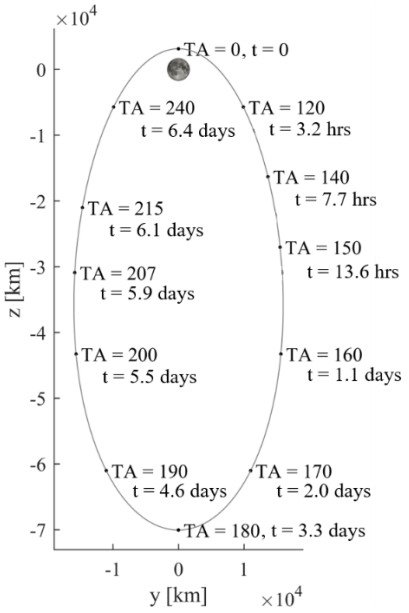

Figure 1. 9:2 NRHO in the CR3BP

The Gateway NRHO is selected as the southern L2 halo orbit in the Earth-Moon system that exhibits a 9:2 resonance with the lunar synodic period. The resonant NRHO is favorable as a long-term orbit for the Gateway as it is nearly stable, and thus requires low orbit maintenance Δv. When phased properly, this NRHO excludes eclipses from the Earth's shadow. Perfectly periodic in the CR3BP, the NRHO exists as a quasi-periodic orbit in the higher-fidelity ephemeris model. A 15-year baseline trajectory carefully designed to avoid long-duration eclipses is available on the JPL NAIF server.[4] This 15-year baseline NRHO is composed of approximately 840 revolutions around the Moon.

The Gateway NRHO as computed in the CR3BP appears in an Earth-Moon rotating view in Figure 1. There are several ways to parameterize a location along the NRHO. One parameter used in the current study is osculating true anomaly, TA, as pictured in Figure 1. Describing locations along the NRHO in terms of TA is useful since it is an intuitive measure familiar from Keplerian dynamics. The NRHO can also be parameterized by time, advantageous when operational planning and execution times are considered. A spacecraft in the NRHO moves quickly near perilune and quite slowly near apolune; while the period of the orbit is 6.56 days, a spacecraft in the NRHO moves from TA = 0° at perilune to TA = 120° in just 3.2 hours. Thus, points spaced equally in time are clustered near apolune, while points spaced equally in TA are clustered near perilune.

The Gateway NRHO is a slightly unstable orbit and, thus, requires regular OM maneuvers. One effective method of maintaining the orbit is an x-axis crossing control algorithm.[3,5] In the current investigation, the OM algorithm is designed to maintain the perilune passage time, or phase, as well as the geometry of the NRHO; maintaining the phase from the baseline NRHO ensures that long-duration eclipses from the Earth's shadow are avoided. Maneuvers are placed each revolution at TA = 200º, about one day prior to perilune passage. A differential corrector is employed to initially design a maneuver that delivers a downstream velocity constrained as

$$v_x = v_{xref} \pm v_{tol} \tag{1}$$

where v_x is the x-component of rotating velocity at the controlled spacecraft's perilune passage in the Earth-Moon rotating frame at some target horizon downstream, v_{xref} is the x-component of rotating velocity along the baseline NRHO at its respective perilune passage, and the tolerance v_{xtol} is set to 0.45 m/s. The targeting horizon is initially set to 6.2 revolutions, so that the rotating x-velocity constraint given in Eq (1) is satisfied at the seventh perilune passage downstream from the maneuver. If the targeter fails to converge, the targeting horizon is reduced successively until convergence is achieved. The resulting Δv is used as an initial guess to subsequently target both v_x and a weighted perilune passage time. The weighting is implemented by defining a target epoch

$$t_{targ} = W_t\left(t_{pref} - t_p\right) + t_p \tag{2}$$

where $W_t = 0.3$ is a weighting factor, t_{pref} is the perilune passage time along the baseline NRHO, and t_p is the perilune passage time achieved by the maintained spacecraft each iteration. The algorithm is then summarized as follows:

Algorithm 1:

- Step spacecraft to TA = 200°
- Target $v_x = v_{xref} \pm 0.45$ m/s at perilune 6.2 revolutions downstream (Eq. 1)
- If convergence fails, reduce targeting horizon until convergence is achieved
- Do not execute maneuver. Use computed Δv as an initial guess to target:
    - $v_x = v_{xref} \pm 0.45$ m/s (Eq. 1) **and**
    - $t_p = t_{targ} \pm 15$ minutes at perilune 6.2 revolutions downstream (Eq. 2)
- If convergence fails, reduce targeting horizon until convergence is achieved
- If $|\Delta v| > 3$ cm/s, execute maneuver. Otherwise skip maneuver.

This algorithm effectively maintains a spacecraft within the NRHO for the full 15 years of the baseline trajectory in the presence of reasonable operational errors. The results of a 2-year, 100-Monte Carlo trial simulation in the ephemeris force model appears in Figure 2. The Δv for each of the 112 revolutions appears in Figure 2a. The magnitudes range from the specified minimum of 3 cm/s to approximately 18 cm/s. The cumulative Δv for each of the trials appears in Figure 2b. The mean Δv to maintain the spacecraft over the 2-year propagation is approximately 2 m/s; the maximum value is 2.6 m/s. Figure 2c and d represent the deltas from the baseline measured at each perilune passage. The difference in perilune passage time between each propagated trial and the baseline NRHO appears in Figure 2c; the phase is maintained, and t_p remains within an hour of the values along the baseline NRHO. While the patterns are obscured by the 100 trials included in Figure 2c, it is apparent when considering single trials that an annual period exists in the t_p differences, though the phase is inconsistent from one trial to the next. Similarly, the differences in the inertial position vectors at perilune between the propagated spacecraft in each trial and the baseline NRHO (as measured at each respective perilune passage) appear in Figure 2d. The Z components of the position differences at perilune dominate, but each position delta remains within approximately 50 km of the baseline trajectory. Note that the simulation illustrated in Figure 2 does not include a DAM or other phase change maneuver.

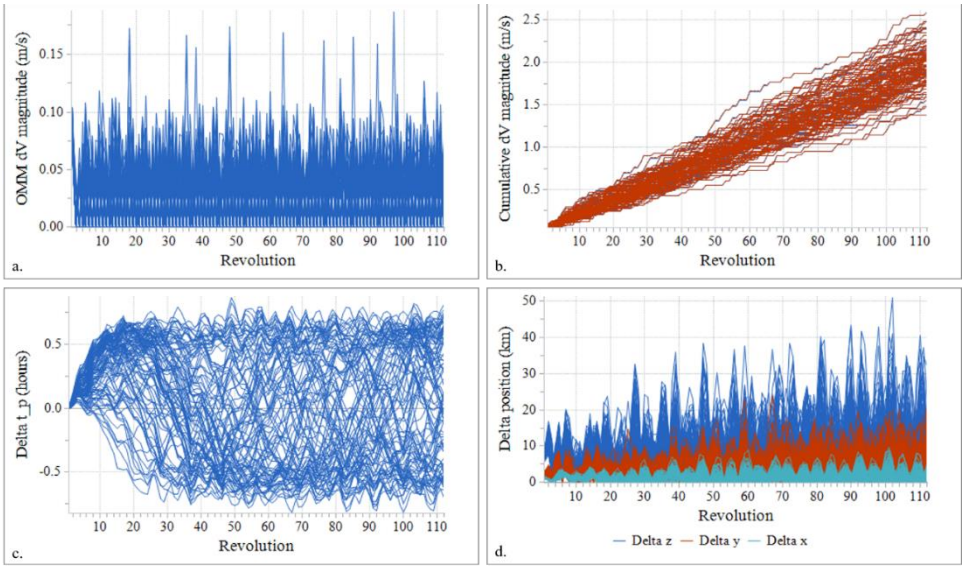

Figure 2. Two years of orbit maintenance in the NRHO without a phase shift or DAM. OM Δ*v* for each revolution (a), cumulative OM Δ*v* (b), delta t_p relative to the baseline NRHO (c), delta position at perilune relative to the baseline NRHO (d).

DEBRIS AVOIDANCE MANEUVERS

During the Gateway's multi-year lifetime, debris objects or other spacecraft may present conjunction risks that necessitate DAM execution. Debris avoidance maneuvers in low Earth orbit are well understood, but the dynamics and challenges in the NRHO differ significantly. Any maneuver executed to avoid a conjunction must be corrected so that the Gateway returns to its original favorable phase within the 9:2 NRHO. In addition, the diverted trajectory should remain nearby the NRHO to ensure the Gateway does not quickly depart the lunar vicinity in the event of a contingency after the initial DAM. Thus, the total DAM cost consists of two components: the Δ*v* cost to avoid the conjunction and the Δ*v* cost to return to the baseline orbit. By selecting dynamically informed maneuver directions, a low-cost strategy is identified for debris avoidance.

Initial DAM Perturbation

The goal of a DAM in the current investigation is to avoid a conjunction and then return to the baseline NRHO. A schematic of the DAM appears in Figure 3. At the initial time, t_0, a DAM Δ*v* is performed to avoid a conjunction at time t_{miss}, diverting the original trajectory by a miss radius, r_{miss}. After a total duration $t_{horizon}$, the diverted trajectory returns nearby to the original path. Thus, the initial Δ*v* is designed to achieve a sufficient separation to ensure collision avoidance. However, the DAM must also keep the diverted trajectory close to the baseline to reduce recovery costs and to prevent departure from the NRHO if subsequent recover burns are missed. To achieve these goals, the magnitude and direction of the initial DAM Δ*v* are determined that will yield a sufficient miss distance while keeping the diverted trajectory close to the original trajectory.

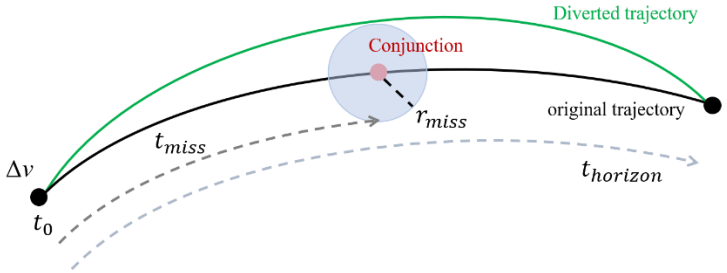

Figure 3. Schematic of the DAM

The initial DAM magnitude is determined using a simple estimate. Given a desired miss distance, r_{miss}, at a specified time, t_{miss}, downstream from the maneuver, the initial DAM Δv is estimated as

$$\Delta v \approx \frac{\Delta r}{\Delta t} \approx \frac{r_{miss}}{t_{miss}} \tag{3}$$

For DAMs outside of the vicinity of perilune, and for relatively small values of r_{miss} and t_{miss}, this linear approximation yields a miss distance near the desired value at the miss time. A table of initial DAM Δv estimates used in this analysis appear in Table 1.

Table 1. Initial DAM Δv estimates

r_{miss} (km)	t_{miss} (hours)	initial DAM Δv (m/s)	r_{miss} (km)	t_{miss} (hours)	initial DAM Δv (m/s)
25	24	0.3	100	12	2.3
50	24	0.6	100	18	1.5
75	24	0.9	100	24	1.2
100	24	1.2	100	30	0.9
150	24	1.7	100	36	0.8
200	24	2.3	100	48	0.6

Next, the Cauchy-Green strain tensor (CGT)[7,6] is employed to compute maneuver directions that yield the smallest separation between the baseline NRHO and the perturbed Gateway after a selected time horizon. The CGT, C, is computed from the state transition matrix (STM), Φ. The STM maps an initial perturbation along a reference path to the final perturbation after a given time horizon such that

$$\delta x(t_f) = \Phi(t_f, t_0)\delta x(t_0) \tag{4}$$

where the initial and final epochs are represented by t_0 and t_f, respectively. Alternatively, the relationship between the initial perturbation and the magnitude of the final perturbation can be written as

$$\left\|\delta x(t_f)\right\|^2 = \delta x(t_0)^T C(t_f, t_0)\delta x(t_0) \tag{5}$$

where the matrix $C(t_f, t_0)$ is computed from the STM as

$$C(t_f, t_0) = \Phi^T(t_f, t_0)\Phi(t_f, t_0) \tag{6}$$

The positive-definite CGT then describes the stretching of the flow in the vicinity of the reference trajectory. An eigen-decomposition of the time-dependent CGT yields the direction of a perturbation that results in the smallest divergence from the reference after a given time horizon, denoted the most-restoring direction, as well as the direction of perturbation than yields the largest departure from the reference after the specified time horizon, i.e, the most-stretching direction. In the current analysis, the goal is to identify the velocity perturbation that yields the smallest separation in position and velocity after a given time horizon. Thus, considering the submatrices of the STM,

$$\Phi(t_f, t_0) = \begin{vmatrix} \phi_{rr} & \phi_{rv} \\ \phi_{vr} & \phi_{vv} \end{vmatrix} \tag{7}$$

the right-hand submatrix, $\begin{bmatrix} \phi_{rv} \\ \phi_{vv} \end{bmatrix}$ maps an initial velocity perturbation to a final position and velocity separation. The most-restoring direction associated with this mapping is defined as the right-singular vector associated with the minimum singular value of the $\begin{bmatrix} \phi_{rv} \\ \phi_{vv} \end{bmatrix}$ submatrix defined by a specified time horizon.

Further details appear in Muralidharan and Howell.[6] In this study, the most-restoring direction is computed in the CR3BP and used in simulations in the higher-fidelity ephemeris force model.

With the initial DAM magnitude and direction selected, the DAM Δv is executed at $t = t_0$. To ensure the desired miss distance is achieved, a differential corrector is used to target r_{miss} after the timespan t_{miss}. The maneuver is iteratively adjusted if the computed miss distance lies outside of a tolerance, set here to 5 km. An example appears in Figure 4. In this example, a DAM is executed at TA = 150º. The miss distance is set to 100 km, and the miss time is set to 24 hours. The range between the original trajectory and the perturbed trajectory is then recorded over 22 days, assuming no further maneuvers are executed. The maneuver magnitude of 1.2 m/s is not adjusted by the targeter in this case since the miss distance is achieved within the tolerance. Over the subsequent 22 days, the perturbed trajectory remains within approximately 800 km of the original trajectory, with maxima at perilune passages, even when no further corrections are made. The selection of the most-restoring direction for the maneuver results in the close proximity of the two trajectories. This initial DAM Δv represents the first portion of the DAM cost – the cost to avoid the conjunction; additional costs arise from the recovery to the baseline NRHO.

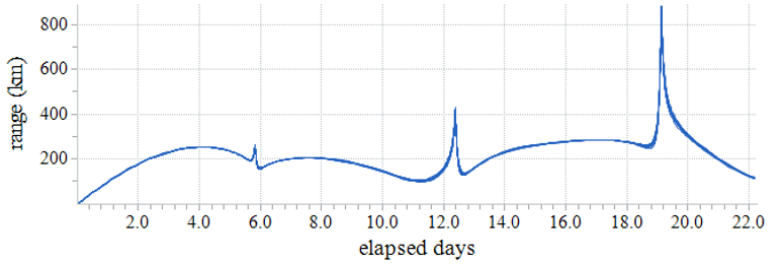

Figure 4. Range between the original trajectory and the perturbed trajectory after a DAM Δv with no post-DAM maneuvers. The DAM achieves a 100 km miss distance after 24 hours and remains nearby the original trajectory for multiple revolutions.

DAM Recovery

After the miss distance is achieved at the specified miss time, the spacecraft must return to the baseline NRHO at the appropriate phase. Because the most-restoring direction is selected for the initial DAM Δv, the perturbed trajectory remains nearby the original NRHO, as illustrated in Figure 4. The proximity in both position and velocity space enables recovery without a dedicated second DAM Δv. Instead, the nominal OM is capable of recovering the perturbed spacecraft to the original trajectory. That is, after the conjunction is avoided, OM resumes at the next opportunity. The second portion of the DAM cost is simply the additional OM Δv required to return the perturbed trajectory close to the baseline NRHO. Recall that the OM algorithm employs values of v_x and t_p from the baseline NRHO as targets. Post-DAM recovery options include applying the standard OM algorithm as previously described; a second option involves augmenting the OM algorithm with additional targets to more effectively return the perturbed spacecraft to the baseline NRHO.

For example, consider a conjunction identified at TA = 163º in the 15th revolution along the NRHO. A DAM is designed to execute 24 hours prior to the conjunction and achieve a miss distance of 100 km. The initial DAM is performed at TA = 142º with a Δv of 1.2 m/s. After the conjunction is avoided, OM resumes at TA = 200º without updates to the OM algorithm. The results of a 2-year simulation including 100 Monte Carlo trials appear in Figure 5. The OM burn immediately after the DAM is apparent at revolution 15 by the increased burn magnitude in Figure 5a. Not that the post-DAM OM burn is never skipped. The cost for the single OM burn exceeds 25 cm/s. However, the OM costs for each maneuver returns to the nominal range (under 18 cm/s) after the post-DAM OM burn. The post-DAM recovery cost is also apparent in the cumulative Δv plot in Figure 5b as a steep increase at revolution 15. The mean OM Δv for the two-year timespan increases by 0.2 m/s as a result of the DAM, from 2.0 m/s without a DAM to 2.2 m/s including DAM recovery. The mean total DAM Δv or 1.4 m/s is a combination of the initial DAM Δv, 1.2 m/s, and the additional OM Δv for recovery, 0.2 m/s.

While the OM Δv costs return to their original levels after the DAM recovery, it is interesting to consider the trajectory differences after the DAM. Recall from Figure 2c that the differences in t_p between each propagated Monte Carlo trial and the baseline NRHO remain under 0.75 hours, with no consistent phase

signature from one trial to the next. By contrast, after the DAM execution, a consistent periodic oscillation appears in the t_p differences, as apparent in Figure 5c. The magnitude of the t_p differences remain within 0.75 hours, however, without secular growth. The position differences at perilune appear in Figure 5d; the post-DAM values are noticeably larger, reaching maximum values over 80 km in Z, however, they do not demonstrate secular growth. The differences from the baseline in perilune passage time and location do not appear to affect the long-term OM cost.

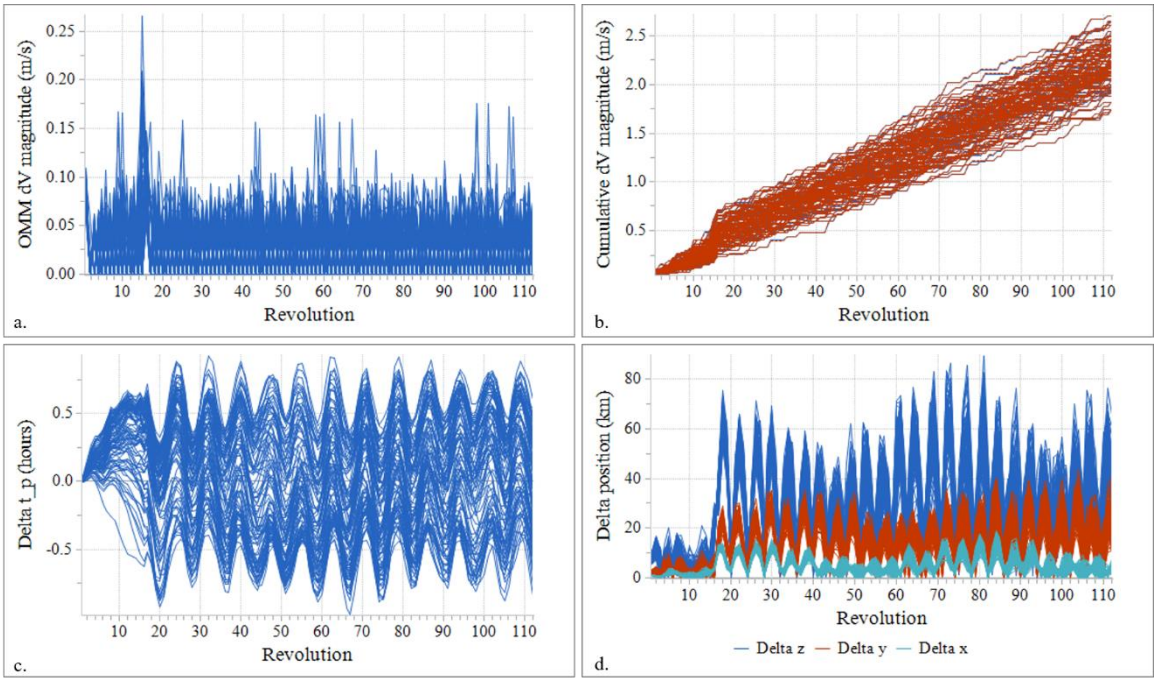

Figure 5. DAM executed at TA = 142° to avoid a conjunction by 100 km after 24 hours. OM Δv each revolution (a), cumulative OM Δv (b), delta t_p relative to the baseline NRHO (c), delta position at perilune relative to the baseline NRHO (d).

It may be desirable to damp the oscillations apparent in the perilune position and timing differences after the DAM, as well as to reduce the magnitude of the post-DAM perilune location differences. Adding additional targets to the OM algorithm for several revolutions after the DAM is one method to achieve this goal. In the current analysis, a third target is added to the OM algorithm: the y-component of the position vector at perilune in the Earth-Moon rotating frame. The augmented post-DAM OM algorithm then becomes:

Algorithm 2:

- Step spacecraft to TA = 200°
- Target $v_x = v_{xref} \pm 0.45$ m/s at perilune 6.2 revolutions downstream (Eq. 1)
- If convergence fails, reduce targeting horizon until convergence is achieved
- Do not execute maneuver. Use computed Δv as an initial guess to target:
  - $v_x = v_{xref} \pm 0.45$ m/s (Eq. 1) **and**
  - $t_p = t_{targ} \pm 15$ minutes at perilune 6.2 revolutions downstream (Eq. 2)
- If convergence fails, reduce targeting horizon until convergence is achieved
- Do not execute maneuver. Use computed Δv as an initial guess to target:
  - $v_x = v_{xref} \pm 0.45$ m/s (Eq. 1) **and**
  - $t_p = t_{targ} \pm 15$ minutes at perilune 6.2 revolutions downstream (Eq. 2) **and**
  - $y = y_{ref} \pm 10$ km at perilune 6.2 revolutions downstream
- If convergence fails, reduce targeting horizon until convergence is achieved
- If $|\Delta v| > 3$ cm/s, execute maneuver. Otherwise skip maneuver.

This augmented OM algorithm (Algorithm 2) is applied for the three OM burns following the initial DAM Δv. After three revolutions, the OM algorithm returns to the original formulation (Algorithm 1) with two targets, perilune passage time and rotating x-velocity. The scenario illustrated in Figure 5 is repeated with the augmented OM algorithm applied; the OM burn history and the trajectory differences at perilune resulting from the 100-trial simulation appear in Figure 6. Of immediate note is the increase in OM Δv for the three revolutions after the DAM that include the y-position target. This increase appears in Figure 6a; the OM Δv can reach nearly 0.9 m/s for the second of these three recovery burns. The increase is also apparent in the cumulative Δv curves in Figure 6b. The mean Δv for the 2-year propagation is approximately 3 m/s, an increase in 0.8 m/s for DAM recovery. However, the extra cost serves to remove the signatures previously observed in the post-DAM trajectory differences. The oscillation noted in the perilune passage time differences in Figure 5c is no longer apparent in Figure 6c. Similarly, the position differences relative to the baseline NRHO, plotted in Figure 6d, remain less than approximately 50 km, as in the case without a DAM in Figure 2d. The post-DAM behavior resembles DAM-free behavior at the cost of approximately 1 m/s in additional Δv.

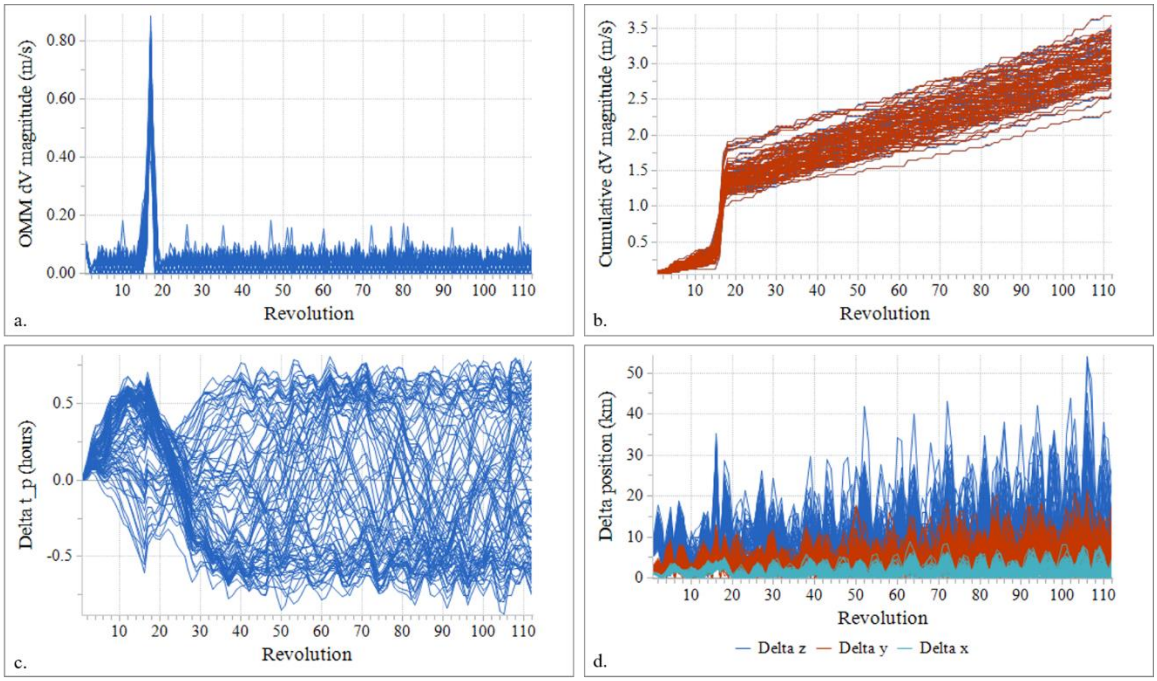

Figure 6. DAM executed at TA = 142° to avoid a conjunction by 100 km after 24 hours with augmented post-DAM OM. OM Δv each revolution (a), cumulative OM Δv (b), delta t_p relative to the baseline NRHO (c), delta position at perilune relative to the baseline NRHO (d).

As discussed, the total cost of a DAM consists of two components. The first component is the initial Δv designed to avoid a conjunction by a radius r_{miss} at a time t_{miss} after the maneuver. These costs are summarized in Table 1. The second contribution to the total DAM cost is the additional post-DAM OM Δv that returns the spacecraft to a state near its original baseline NRHO, either with or without the damping of post-DAM oscillatory signatures in the perilune position and timing differences. Characterizing the costs for all potential DAM situations is challenging due to the size of the design space. Costs and effectiveness vary with miss distance, miss time, initial DAM location along the NRHO, epoch of the revolution within the NRHO, and selected strategy. However, a preliminary characterization of the design space is performed here to serve as a baseline for cost estimates and strategy evaluation. First, the variations in OM Δv are assessed as a function of DAM location along the NRHO for various values of miss time. The 2-year OM costs for an uncrewed spacecraft in the Gateway NRHO appear in Figure 2. If no DAM is executed, the mean OM Δv based on 100 Monte Carlo trials is approximately 2 m/s; this value appears in purple. The mean total OM Δv for the same

2-year period increases if a DAM is executed. Figure 2a illustrates the OM costs assuming *y*-targets are added to the OM algorithm for 3 revolutions after the DAM to suppress the oscillations in the post-DAM trajectory differences. In Figure 2b, the same costs appear when the oscillations are not damped, and the nominal OM algorithm remains unadjusted. In all cases, the miss distance is set to 100 km. The costs for miss times of 12, 24, and 36 hours are marked in orange, blue, and yellow respectively. Each datapoint represents the mean value after 100 Monte Carlo trials. In the current analysis, each DAM is implemented without maneuver execution error. Several patterns are immediately apparent. Unsurprisingly, the additional OM costs decrease with increasing miss time. For t_{miss} = 12 hours, the algorithms are effective for a DAM location range such that 100º < TA < 210º; closer to perilune, the current OM algorithm is unable to successfully target the post-DAM OM maneuver. For longer miss times, DAM execution is available for a wider band of TA values; both algorithms succeed through TA = 293º with 24 and 36-hour miss times. In every case, a local minimum in cost is observed for a DAM executed at apolune, at TA = 180º. For miss distances of 24 and 36 hours, a second minimum is observed for DAMs executed near the location of the OM maneuver itself, TA = 200º. As the DAM location traverses the NRHO and the miss time is adjusted, the relative placement of the DAM and the conjunction with respect to nearby OM burns must be considered. For example, if an OM maneuver at TA = 200º is located between the DAM and the miss time, the OM burn is skipped until the next revolution. In this analysis, if a DAM is located immediately after an OM maneuver, the OM burn is not skipped, though in practice, the operations team would surely consider combining the OM and the DAM.

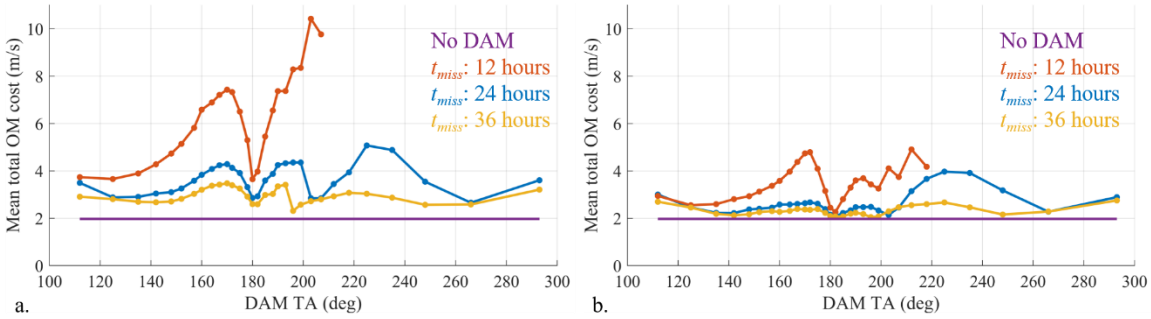

Figure 7. Mean total OM Δ*v* for two years in the NRHO as a function of DAM TA for 12, 24, and 36-hour miss times and a 100 km miss distance. With added *y*-targets after the DAM (a), without added *y*-targets after the DAM (b). Baseline OM cost for 2-year propagation in purple.

It is apparent from the two plots in Figure 7 that including the additional *y*-target in the OM algorithm after the DAM to damp the oscillations in the post-DAM trajectory differences relative to the baseline NRHO increases the cost of the post-DAM cleanup. The cost differences between the two algorithms appear in Figure 8. For a miss time of 24 hours, the maximum difference in cost reaches 2 m/s for a DAM performed at TA = 199º, immediately prior to the next scheduled OM maneuver, in which case the OM burn is skipped until the next revolution. For a miss time of 36 hours, on the other hand, the difference in cost between the two algorithms generally remains under 1 m/s. For a smaller miss time of 12 hours, damping the oscillations adds over 1 m/s in nearly every case, and the additional costs can exceed 6 m/s. Given that the total two-year OM cost is just 2 m/s when no DAM is executed, a 6 m/s difference between two algorithms is significant. These cost differences may determine if it is worthwhile to damp the post-DAM oscillations in position and t_p differences with respect to the baseline NRHO.

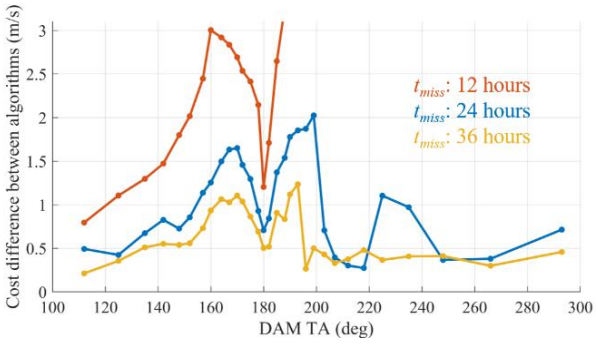

Figure 8. Cost difference between the two post-DAM OM algorithms

As the miss time and miss distance change for a given DAM location, the DAM recovery costs also vary. Initial DAM Δ*v* perturbations increase with decreasing miss times or increasing miss distances, as estimated in Table 1. Thus, it is

unsurprising that correcting for a larger perturbation demands larger post-DAM OM Δv. To demonstrate the OM cost dependency on initial DAM Δv, t_{miss} and r_{miss} are separately varied and 100 Monte Carlo trials run with each OM algorithm. Given a 100 km miss distance and a DAM location at TA = 142°, the miss time is varied from 12 hours to 54 hours in Figure 9a. Costs decrease for both algorithms as miss time increases, reaching a steady minimum for miss times over 36 hours. Similarly, the miss distance is varied given a 24 hour miss time and DAM location of TA 142° in Figure 9b. As expected, the recovery costs grow as the miss distance increases, since the initial DAM perturbation is larger. The results in Figure 9 demonstrate advantages when the ephemeris of the debris object is well known and a smaller miss distance and/or longer miss time can be selected to ensure spacecraft safety. In these cases, both the initial DAM Δv and the post-DAM recovery costs are lower.

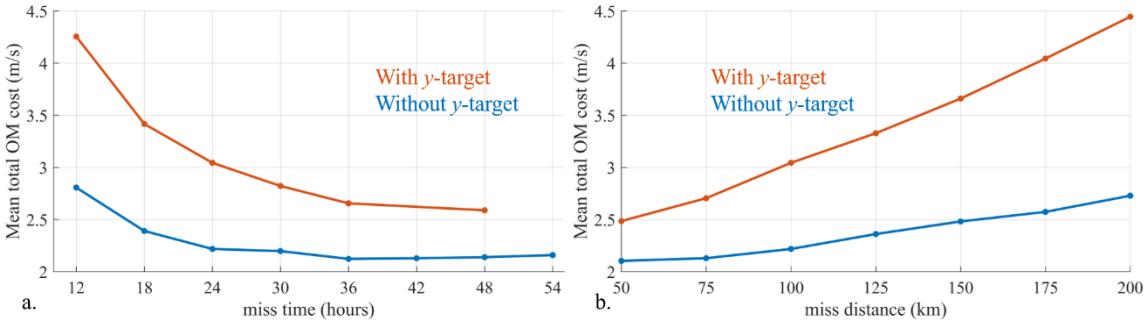

Figure 9. Mean total OM Δv for two years in the NRHO as a function of miss time for a 100 km miss distance (a) and miss distance for a 24-hour miss time (b) for a DAM executed at TA = 142°

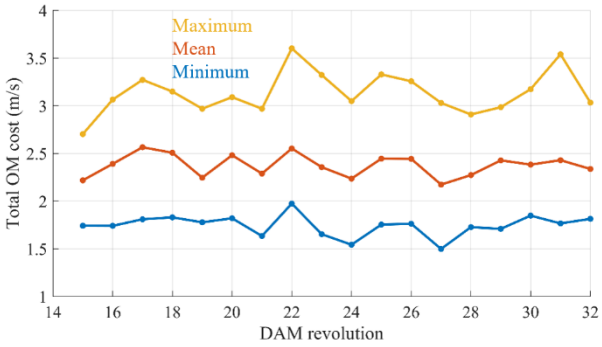

Figure 10. Minimum, mean, and maximum OM Δv for two years in the NRHO as a function of DAM revolution for a 100 km miss distance, a 24-hour miss time, and DAM TA = 142° without augmented OM targets

Finally, the post-DAM recovery costs vary according to the epoch of the DAM, or, equivalently, the revolution along the baseline NRHO during which the DAM is executed. The minimum, mean, and maximum total OM Δv appears in Figure 10 for a DAM executed at TA = 142° for 18 consecutive revolutions along the baseline NRHO. In each case, the miss distance is set to 100 km and the miss time to 24 hours. Each datapoint represents 100 Monte Carlo trials without *y*-targets included in the post-DAM OM algorithm. The mean values vary by approximately 0.4 m/s as the DAM revolution is changed. For a given revolution, the spread between the minimum and maximum costs over the 100 trials ranges from 1 – 1.8 m/s.

In summary, two algorithms are successfully demonstrated to achieve low-cost DAM execution and recovery by applying an initial Δv in a most-restoring direction and then resuming orbit maintenance at the next opportunity, one with and one without additional targets to reduce trajectory differences from the baseline NRHO. Employing the most-restoring direction is crucial to the success of these algorithms, as the dynamically informed direction ensures the perturbed spacecraft returns sufficiently near to its baseline trajectory to enable the OM algorithms to successfully recover the original orbit. It is important to note that this analysis does not consider the trajectory of the debris object or whether the DAM may lead to future conjunctions, and it does not consider how knowledge of the debris object is acquired. Likewise, the uncertainties associated with the state knowledge of the maneuvering spacecraft and the debris object remain unaccounted for. This analysis is a first look at the strategies and costs associated with performing a maneuver with short notice to avoid a conjunction by a certain miss distance. The total cost of a given DAM is a combination of the initial DAM Δv and the additional OM cost to recover from the perturbation.

PHASE CHANGES FOR MISSION OPPORTUNITIES

The Gateway baseline NRHO is carefully aligned in phase to avoid long eclipses from the Earth's shadow.[4] However, it may be desirable to temporarily change phase within the 9:2 NRHO to enable mission opportunities or facilitate rendezvous with a visiting vehicle. In such a scenario, a plan for the phase change would be in place well in advance of the rendezvous. Thus, in contrast to the debris avoidance maneuver occurring with only hours or days of notice, a long-lead phase change can be executed over the course of weeks or months. Similar to the DAM strategy, a long-lead phase change strategy is proposed that employs the orbit maintenance algorithm to adjust the phase of Gateway over the course of many revolutions. In comparison to a two-burn transfer that changes phasing within one revolution of the NRHO, this long-lead approach reduces the overall cost of the phase change.[7]

Recall that OM Algorithm 1 employs both the x-component of rotating velocity and the perilune passage time as targets in a differential corrector. The long-lead phase change strategy simply adjusts the perilune passage time target incrementally to achieve a desired phase shift after a specified number of revolutions. Then, after a certain number of revolutions held at the new phase, the process is reversed to return to the original phase within the NRHO. That is, the time target defined in Equation 2 is adjusted so that

$$t_{targ} = W_t\left(t_{pref} + \Delta t - t_p\right) + t_p \tag{8}$$

where the value of Δt is function of the number of revolutions over which to execute the phase shift, N, and the magnitude of the total phase shift desired, t_{shift}. For each revolution, i, during the phase shift process, Δt is defined as

$$\Delta t = i\frac{t_{shift}}{N} \tag{9}$$

Equation 2 in the OM algorithm is replaced with Equation 8 for the duration of the phase shift. A schematic of the phase shift appears in Figure 11, with the magnitude of the phase shift, t_{shift}, and the number of revs over which the shift is executed, N, noted.

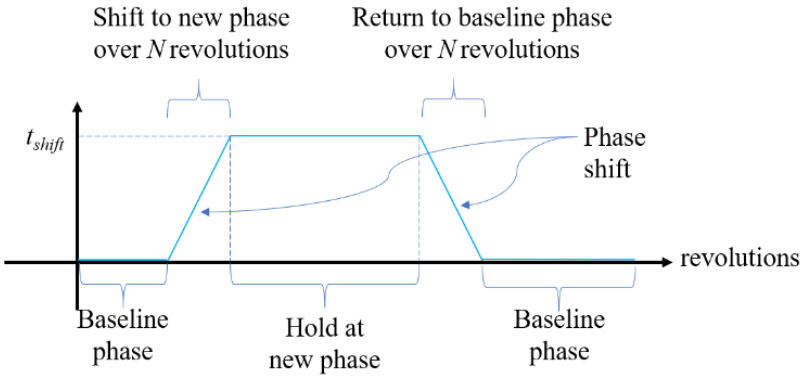

Figure 11. Schematic of the long-lead shift to a desired phase and back to the baseline.

An example appears in Figure 12 for 100 Monte Carlo trials simulating an initial phase shift t_{shift} = 10 hours over N = 10 revolutions. After holding at the new phase for 20 more revolutions, or about 4 months, the spacecraft reverses the process to return to the baseline phase over N = 10 revolutions. Then, OM is performed as in Algorithm 1 to complete a 2-year (112-revolution) propagation. Several notable differences are apparent in a comparison with the baseline example with no phase shift from Figure 2. The magnitude of each OM maneuver in the simulation appears in Figure 2a. The OM Δv magnitudes during the phase shift and the hold at the new phase are larger than observed in nominal OM, reaching a maximum value over 0.45 m/s. After the return to the baseline phase, the magnitudes of the OM burns return to a steady state, albeit with a slightly larger magnitude than the nominal cases illustrated in Figure 2. The higher OM costs during the phase shift are also apparent in the steeper slope of the cumulative Δv in Figure 2b. The mean total Δv for the 2-year propagation including the 10-hour phase shift (and return) is 6.4 m/s, in increase of 4.4 m/s

over the baseline 2-year OM cost. The phase shift itself is visible in the perilune passage time deltas relative to the baseline NRHO plotted in Figure 2c. The desired phase shift of 10 hours is achieved is achieved within ±1 hour of the target, t_{shift}, and is held for 20 revolutions; the phase is then shifted back to the baseline, returning to its initial phase at approximately revolution 60, just over a year after the start of the simulation. Note the oscillations in the t_p deltas after the phase is returned to the baseline; this oscillation, with a magnitude less than 1 hour and no secular trend, is reminiscent of the oscillations seen after a DAM in Figure 5. Similarly, the variations in position at perilune relative to the baseline NRHO are apparent in Figure 2d. While the oscillations are not growing, they may be undesirable and may lead to increased OM costs over the long term.

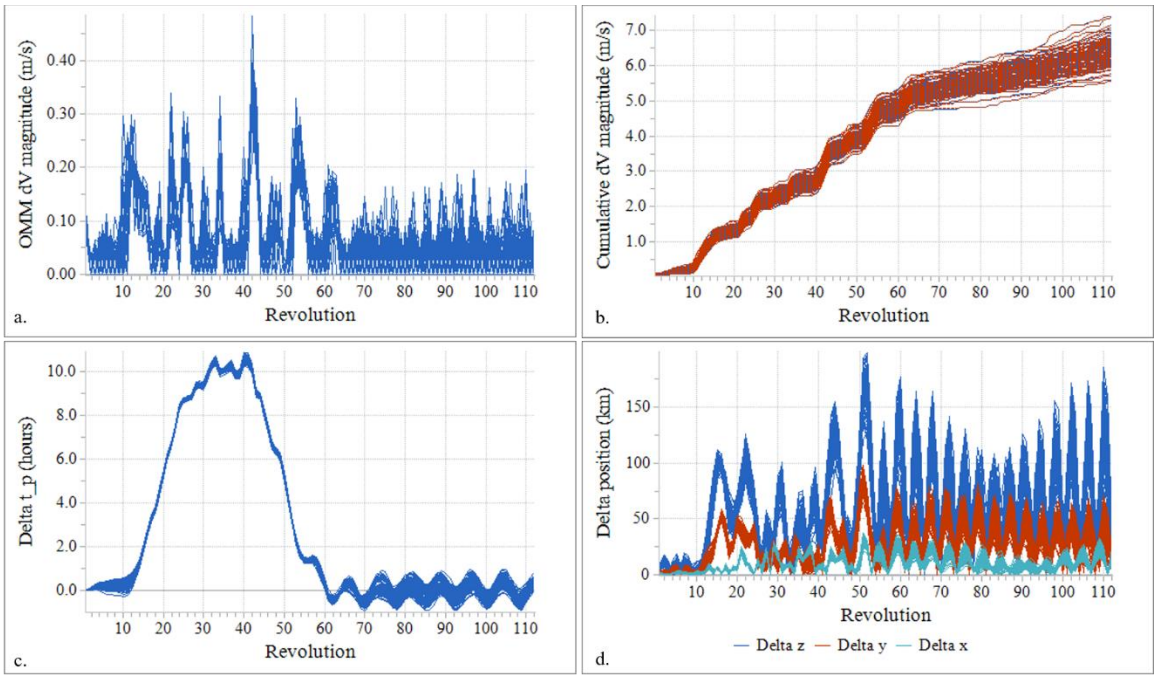

Figure 12. Phase shift of 10 hours over 10 revolutions. OM Δ*v* each revolution (a), cumulative OM Δ*v* (b), delta t_p relative to the baseline NRHO (c), delta position at perilune relative to the baseline NRHO (d).

As in the case of the DAM algorithm, if the oscillations observed in the timing and state variations at perilune relative to the baseline NRHO are deemed undesirable, they can be damped by adding a target to the OM algorithm. As before, the OM algorithm is augmented by additionally targeting the *y*-position coordinate in Earth-Moon rotating coordinates algorithm for three revolutions after returning to the baseline phase; this strategy is denoted Algorithm 2. The effectiveness of applying Algorithm 2 for three revolutions is demonstrated in Figure 13. Several sequential large OM maneuvers are executed when the *y*-target is added, reaching a magnitude of 3 m/s, as observed in Figure 13a. While not apparent at this scale, after the large recovery burns, the OM burn magnitudes return near the original values as in Figure 2. A steep increase in the cumulative Δ*v* is noted in Figure 13b associated with the large recovery maneuvers. However, as desired, the periodic oscillation in the perilune passage time deltas depicted in Figure 12c is diminished in Figure 13c, and, after the return to the baseline phase, the magnitudes of the position deltas in Figure 13d are reduced to be nearer the nominal values. The mean total Δ*v* for the 2-year propagation including the 10-hour phase shift (and return using Algorithm 2) is approximately 8.3 m/s, an increase of 6.3 m/s over the baseline 2-year OM cost and an increase of 1.9 m/s over the scenario depicted in Figure 12. Note, however, that the larger correction burns executed upon returning to the baseline phase serve to return the spacecraft closer to the baseline NRHO, and over longer propagations, the resulting reduced OM costs compensate for the larger initial recovery cost.

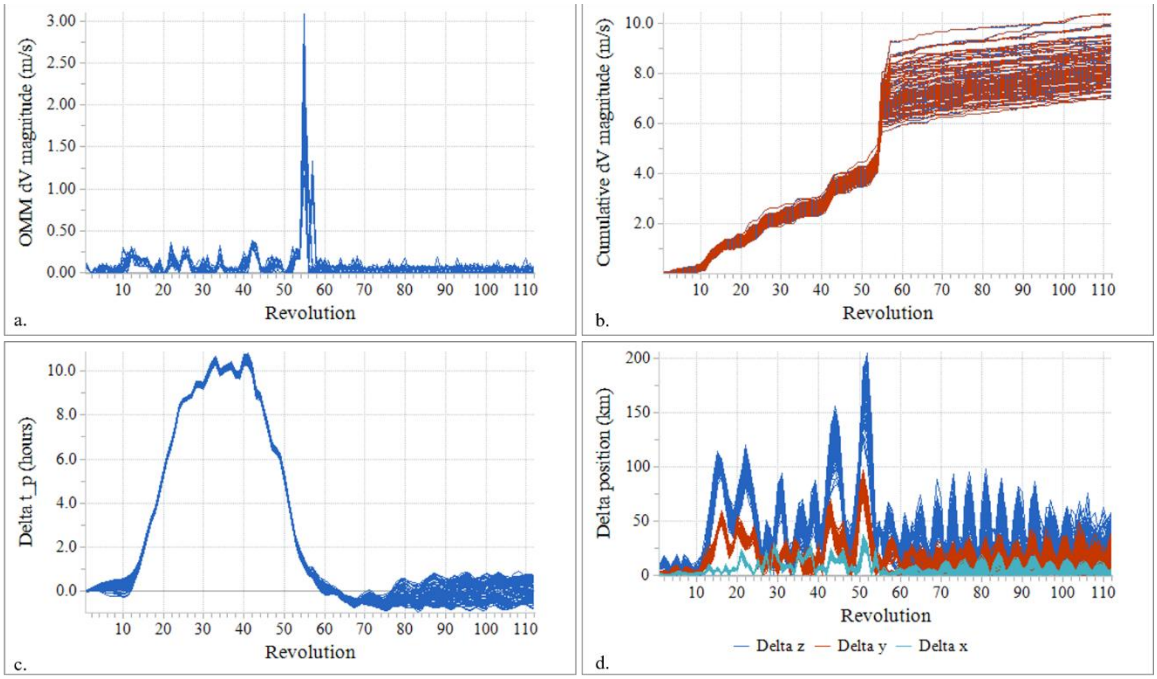

Figure 13. Phase shift of 10 hours over 10 revolutions with OM augmentation after return to baseline. OM Δv each revolution (a), cumulative OM Δv (b), delta t_p relative to the baseline NRHO (c), delta position at perilune relative to the baseline NRHO (d).

Plots of perilune passage time deltas for longer, five-year simulations aid in illustrating the effectiveness of the two OM-based strategies to shift to a new phase and subsequently return to the baseline. Two such cases appear in Figure 14. In these scenarios, the baseline phase is initially held for the first 40 revolutions, or approximately 260 days. Then, a phase shift of $t_{shift} = 10$ hours is executed over $N = 10$ revolutions. After the phase change is complete, the shifted phase is held for 50 revolutions, or about 11 months, prior to returning to the nominal phase over the course of $N = 10$ revolutions. The nominal phase is then targeted for the final 170 revolutions in each trial (approximately 3 years). The simulation results plotted in Figure 14a result from applying the augmented OM algorithm (Algorithm 2) for three revolutions after the phase shift is complete to damp out the oscillatory signature. The results in Figure 14b, on the other hand, employ Algorithm 1 throughout: the same scenario is run without including the additional y-targets after the return to the nominal please. The oscillations in the t_p deltas relative to the baseline NRHO remain apparent in this case. In both cases in Figure 14, the nominal phase is maintained relative to the nominal within approximately 1 hour in the three steady-state portions of the simulation: prior to the phase shift, during the hold at the shifted phase, and after the return to the baseline phase. Notably, secular growth is not observed, even when the oscillations are not damped out.

Recall that in the 2-year simulations illustrated in Figure 12 and Figure 13, the mean OM costs for the 2 years, including the phase shift, are larger by approximately 1.9 m/s when Algorithm 2 is applied to damp out the oscillations after the return to the nominal phase. Recall also that the magnitudes of the OM burns after the return to the nominal phase are smaller when the oscillations are damped. In the longer simulations illustrated in Figure 14, the larger cost of the recovery burns after the return to the nominal phase when the oscillations are damped out are more than compensated by the lower long-term OM costs. The total 5-year cost for OM, including the phase shift, is 10.4 m/s in Figure 14a when the oscillations are damped; the total cost is 10.9 m/s in Figure 14b, when the oscillations remain undamped. In short, the added cost of damping the oscillations and returning to the baseline is worthwhile if the original baseline NRHO will be used for long-term targeting after the return to the baseline phase.

Apparent in both cases in Figure 14, the shift to the new phase appears to begin slightly before the phase-shift commencement at revolution 40. Since the targeted values of v_x and t_p within the OM algorithm are associated with states 6.2 revolutions downstream, OM maneuvers as early as revolution 34 use shifted

perilune passage time targets. However, the nominal phase is maintained within a 1-hour tolerance up until revolution 40, as desired. Similarly, note that a steady state at the new, shifted phase is reached at approximately revolution 57. Since a weighted perilune passage time is used within the targeter, the new phase is achieved with a delay. Again, however, by revolution 50, the targeted phase is achieved to within approximately 1 hour of the baseline, as targeted. The combination of targeting states associated with perilune passage 6.2 revolutions downstream and a weighted perilune passage time drives the delta t_p trends seen in Figure 14. However, this strategy does indeed encourage convergence for a low dV.

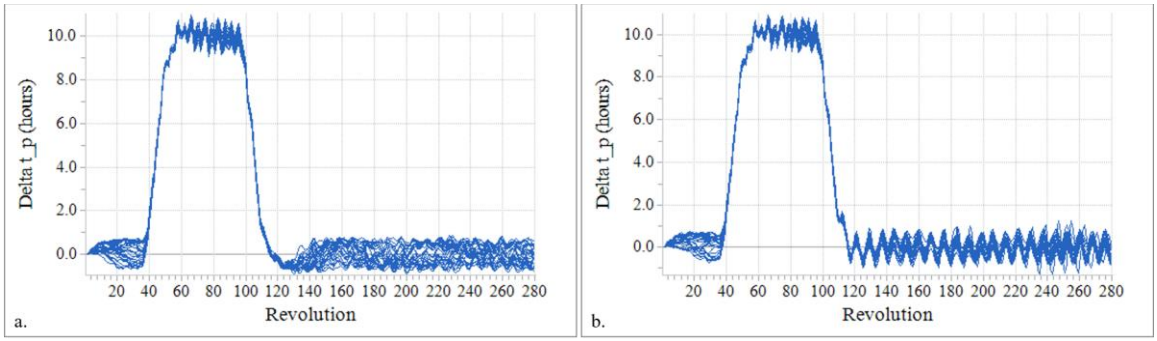

Figure 14. Phase shift of 10 hours over 10 revolutions with (a) and without (b) OM augmentation after return to baseline. 50-revolution hold at the new phase with a 5-year total propagation time.

The simulations depicted in Figure 12 and Figure 13 illustrate scenarios where $N = 10$ revolutions and $t_{shift} = 10$ hours, thus $\Delta t = 1$ hour/revolution. By modifying the number of revolutions over which a phase shift occurs, N, and maintaining the desired shift size, t_{shift}, the effect of shift rate for a given shift size is observed. The minimum, mean, and maximum total OM Δv appears in Figure 15 for various values of N and a 10-hour phase shift. Note that in each scenario, Algorithm 2 is used to return the spacecraft to the nominal phase to reduce the oscillatory signature seen in the perilune passage time deltas and position deltas. Each data point represents 100 Monte Carlo trials with each trial spanning 2 years in the NRHO. In each case, 15 revolutions at the nominal phase using the standard OM strategy (Algorithm 1) are included prior to the start of the phase shift. The mean OM Δv cost decreases with increasing N; the smaller the shift rate, Δt, for a given t_{shift}, the lower the cumulative cost. However, in the current analysis, the total cost is not observed to reduce to that of the nominal scenario depicted in Figure 2 in which there are no DAMs or phase-changes. The difference between the maximum and minimum total OM Δv cost also decreases with increasing N. It can be deduced that slower phase shifts may be more robust to operational errors, thus the total OM cost is more consistent between Monte Carlo trials.

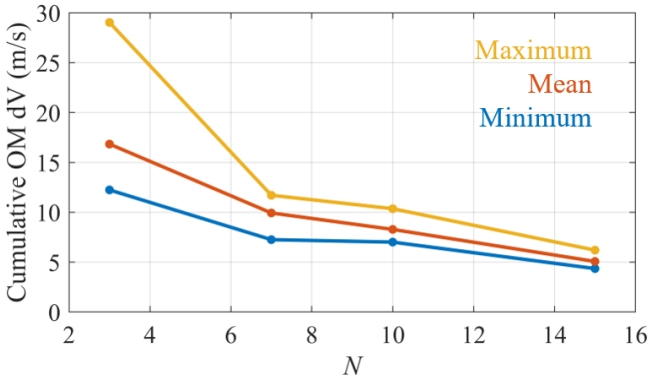

Figure 15. Total 2-year OM cost for phase shift of 10 hours over N revolutions with OM augmentation (Algorithm 2) after return to the baseline.

Alternatively, the relationship between shift rate and total OM cost is investigated by holding N fixed and varying the desired shift size. In Figure 16, the minimum, mean, and maximum OMM costs over two years are plotted for simulations in which $N = 3$ revolutions and t_{shift} is varied. As t_{shift} increases while N is held constant, the shift rate, Δt, increases. Consistent with the trend highlighted in Figure 15, as the shift rate increases, the OM costs also increase. In cases with larger phase shifts, Algorithm 2, as written, is not always able to successfully damp out oscillations that occur after the return to the baseline phase. The larger spread between the minimum and maximum cumulative OM Δv curves illustrates this behavior.

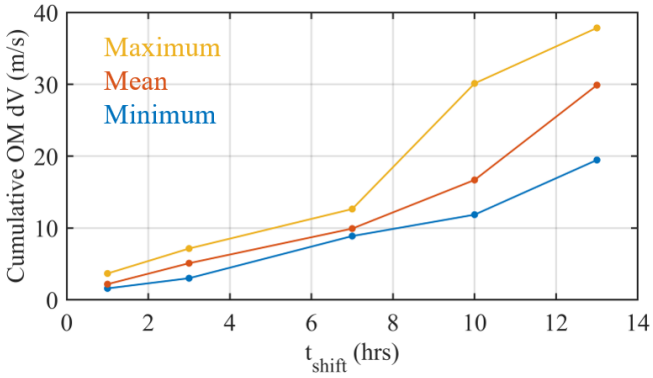

Figure 16. Total 2-year OM cost for phase shift of t_{shift} hours over 3 revolutions with OM augmentation (Algorithm 2) after return to the baseline.

In this investigation, phase shifts of up to 3.275 days, or a half period of the 9:2 NRHO, are simulated. This half-period phase shift moves the spacecraft to an alternate phasing that avoids long-duration eclipsing as in the baseline orbit. Shifting to this new phase using the OM algorithm and a shift rate of approximately 1 hour per revolution successfully achieves the phase shift, however, challenges on returning to the nominal phase are observed, suggesting alternative augmentations of the OM algorithm may be necessary. For smaller phase shifts between 1 and 24 hours, a shift rate of 1 hour per revolution within the phase shift algorithm demonstrates successful phase changes and the ability to return to nominal using the same algorithm. A faster phase shift may be desired to avoid many weeks or months where the spacecraft is not near the baseline NRHO, however, as illustrated in Figure 15 and Figure 16, an increased OM cost may result. In the current analysis, the same baseline NRHO is used as a catalog of targets throughout the process; however, employing a second baseline at the new phase and switching between the two halfway through the process may improve the results. Alternative augmented OM algorithms, including a strategy with progressively tighter tolerance on the additional y-targets, indicate that further reduction of perilune passage time errors and deltas in position after the return to the nominal phase are possible. These further error reductions may require increased OM Δv during the revolutions with additional targets.

CONCLUDING REMARKS

This investigation considers costs and strategies for adjusting the phase of a spacecraft operating in a 9:2 lunar synodic resonant NRHO. First, a strategy is developed to avoid a conjunction and return to the baseline NRHO with only hours or days of notice. By performing the initial DAM Δv in a most-restoring direction based on the CGT, the diverted trajectory naturally returns to the vicinity of the original baseline NRHO, and either the standard or an augmented OM algorithm successfully recovers the pre-DAM behavior. Then, a long-lead phase change strategy is developed to gradually shift the phase of the spacecraft within the NRHO over the course of several or many revolutions. With sufficient lead time, a phase shift is achievable without dedicated maneuvers by adjusting the OM targets. Many additional strategies likely also exist to achieve phase changes for DAMs or to enable mission opportunities. The current analysis investigates methods that employ the current orbit maintenance strategy along with dynamical understanding of the NRHO to adjust the Gateway orbit. Other methods may satisfy additional constraints.

ACKNOWLEDGMENTS

The authors would like to thank Rolfe J. Power for insightful discussions. Portions of this work were completed at NASA JSC and Purdue University through contract #NNJ13HA01C and grant #80NSSC18M0122, respectively.

REFERENCES

[1] Gates, M., M. Barrett, J. Caram, V. Crable, D. Irimies, D. Ludban, D. Manzell, and R. Ticker, "Gateway Power and Propulsion Element Development Status," 69th International Astronautical Congress, Bremen, Germany, October 2018.

[2] Zimovan, E., K. C. Howell, and D. C. Davis, "Near Rectilinear Halo Orbits and Their Application in Cis-Lunar Space," 3rd IAA Conference on Dynamics and Control of Space Systems, Moscow, Russia, May-June 2017.

[3] Davis, D. C., F. S. Khoury, and K. C. Howell, "Phase Control and Eclipse Avoidance in Near Rectilinear Halo Orbits," AAS Guidance, Navigation, and Control Conference, Breckenridge, Colorado, February 2020.

[4]Lee, D.E., "Gateway Destination Orbit Model: A Continuous 15 Year NRHO Reference Trajectory," NASA Johnson Space Center White Paper, August 20, 2019.
[5] Guzzetti, D., E. M. Zimovan, K. C. Howell, and D. C. Davis, "Stationkeeping Methodologies for Spacecraft in Lunar Near Rectilinear Halo Orbits," AAS/AIAA Spaceflight Mechanics Meeting, San Antonio, Texas, February 2017.
[6]Muralidharan, V. and K. C. Howell, "Leveraging stretching directions for stationkeeping in Earth-Moon halo orbits," Advances in Space Research, In Press, October 2021.
[7] Capannolo, A., M. Lavagna, "Minimum Cost Relative Dynamics in Cislunar Environment," 71st International Astronautical Congress, Virtual, September 2020.